THE JOURNAL OF BIOLOGICAL CHEMISTRY VOL. 290, NO. 29, pp. 17656–17667, July 17, 2015

The Neurexin/*N*-Ethylmaleimide-sensitive Factor (NSF) Interaction Regulates Short Term Synaptic Depression*◆

Received for publication, February 9, 2015, and in revised form, April 24, 2015 Published, JBC Papers in Press, May 7, 2015, DOI 10.1074/jbc.M115.644583

Tao Li‡, Yao Tian‡, Qian Li‡, Huiying Chen‡, Huihui Lv‡, Wei Xie‡§, and Junhai Han‡§1

From the ‡Institute of Life Sciences, Key Laboratory of Developmental Genes and Human Disease, Southeast University, Nanjing 210096 and the §Co-innovation Center of Neuroregeneration, Nantong University, Nantong, JS 226001, China

Background: Neurexins (NRXs) are cell adhesion molecules and regulate synapse formation and synaptic transmission.
Results: NRX associates with NSF *in vivo*, and the absence of NRX/NSF interaction results in abnormal distribution and impaired function of NSF.
Conclusion: NRX/NSF interaction facilitates NSF recruitment and subsequent SNARE complex disassembly.
Significance: Neurexin regulates the presynaptic exocytotic machinery.

Although Neurexins, which are cell adhesion molecules localized predominantly to the presynaptic terminals, are known to regulate synapse formation and synaptic transmission, their roles in the regulation of synaptic vesicle release during repetitive nerve stimulation are unknown. Here, we show that *nrx* mutant synapses exhibit rapid short term synaptic depression upon tetanic nerve stimulation. Moreover, we demonstrate that the intracellular region of NRX is essential for synaptic vesicle release upon tetanic nerve stimulation. Using a yeast two-hybrid screen, we find that the intracellular region of NRX interacts with *N*-ethylmaleimide-sensitive factor (NSF), an enzyme that mediates soluble NSF attachment protein receptor (SNARE) complex disassembly and plays an important role in synaptic vesicle release. We further map the binding sites of each molecule and demonstrate that the NRX/NSF interaction is critical for both the distribution of NSF at the presynaptic terminals and SNARE complex disassembly. Our results reveal a previously unknown role of NRX in the regulation of short term synaptic depression upon tetanic nerve stimulation and provide new mechanistic insights into the role of NRX in synaptic vesicle release.

Neurexins are cell adhesion molecules that are thought to be the key presynaptic organization molecules involved in synaptogenesis, synaptic transmission, and synapse maintenance (1–6). The extracellular region of the NRX molecule binds to Neuroligins (7, 8), Dystroglycan (9), Neurexophilin (10–12), leucine-rich repeat proteins (LRRTM2) (13, 14), and Cerebellin (15). In contrast, the intracellular region of the NRX molecule associates with several molecules involved in the synaptic vesicle exocytosis machinery, including synaptotagmin (16) and the PDZ domain-containing proteins CASK (17), Mints (18), and syntenin (19). The neuroligins are localized to the postsynaptic densities (20) and are associated with the neurotransmitter receptors (21, 22). The trans-synaptic interaction of NRX and Neuroligin therefore bridges the synaptic cleft to align the presynaptic neurotransmitter release machinery with the postsynaptic neurotransmitter receptors. Previous studies have shown that the α-NRXs functionally couple Ca^{2+} channels to the presynaptic machinery to mediate synaptic vesicle exocytosis (6). The loss of the single α-NRX in *Drosophila* leads to impaired evoked synaptic transmission and reduced quantal content (4).

Neurotransmitter release is mediated by the fusion of synaptic vesicles, which is triggered by Ca^{2+} and executed by soluble NSF[2] attachment protein receptors (SNAREs). During fusion, vesicular and target SNAREs assemble into an α-helical trans-SNARE complex that forces the two membranes together to form a highly stable SDS-resistant 7S SNARE complex (24–26). After fusion, soluble NSF attachment proteins (SNAPs) bind to SNAREs and then mediate the binding with the ATPase NSF (25), which mediates the disassembly of SNARE complexes and regenerates free SNAREs to be used in subsequent fusion reactions (27). Live image studies have shown that NSF mutant (*i.e. comt*) synapses exhibit defective NSF re-distribution during tetanic nerve stimulation (28), suggesting some potential mechanisms to restrict the mobilization of NSF. However, the molecular mechanism to restrict the mobilization of NSF is not clear.

Here, we show that the *Drosophila* homolog of α-NRX interacts with NSF at the presynaptic terminals. The absence of this interaction in *nrx* mutant synapse leads to rapid short term synaptic depression during tetanic nerve stimulation. We further demonstrate that the NRX/NSF interaction facilitates NSF recruitment to the presynaptic terminals and promotes SNARE complex disassembly. Our results therefore reveal a novel role of NRX in the regulation of short term synaptic depression and an unknown linkage between NRX and the presynaptic exocytotic machinery.

* This work was supported by Ministry of Science and Technology Grants 2014CB942803 and 2012CB517903, Research Project of Chinese Ministry of Education Grant 113028A, Excellent Youth Foundation of Jiangsu Province of China Grant BK20140024 (to J. H.), and National Natural Science Foundation of China Key Program 30930051 (to W. X.). The authors declare that they have no conflicts of interest with the contents of this article.
◆ This article was selected as a Paper of the Week.
[1] To whom correspondence should be addressed: Institute of Life Sciences, Southeast University, 2 Sipailou Rd., Nanjing 210096, China. Tel.: 86-25-83790962; Fax: 86-25-83790962; E-mail: junhaihan@seu.edu.cn.

[2] The abbreviations used are: NSF, *N*-ethylmaleimide-sensitive factor; EJC, excitatory junction current; MBP, maltose-binding protein; NMJ, neuromuscular junction.

Experimental Procedures

Fly Genetics—The flies were maintained on a standard medium at 25 °C with 60–80% relative humidity. The wild-type flies used in this study were w^{1118}. The α-*nrx* (*CG7050*) null mutant allele, nrx^{273}, was obtained from Dr. Manzoor A. Bhat's laboratory (4). The other α-*nrx* null mutant allele, $nrx^{\Delta 83}$, was generated by p-element imprecise excision using Δ2–3 as a transposase source according to standard procedures. The detailed experimental process has been described in a previous report (3). To eliminate potential genetic background effects, the recombinant of two out-crossed *nrx* null mutant alleles, $nrx^{\Delta 83}/nrx^{273}$, was used in this study. To generate the NRX transgenes, the full-length NRX cDNAs and the cDNAs that encode either the C-terminally truncated $NRX^{\Delta C}$ or the PDZ-binding motif-deleted $NRX^{\Delta 4}$ were subcloned into the pUAST vector and injected into w^{1118} flies.

Antibodies—The anti-NSF antibody was generated against a purified GST-NSF (amino acids 1–746) fusion protein in rabbits. An affinity column, which was created by coupling MBP-NSF fusion protein to CNBr-activated Sepharose 4B, was used to purify the antibody. The anti-NRX and anti-Ecp antibodies were generated as described previously (29, 30). Other antibodies were obtained from Developmental Studies Hybridoma Bank (syntaxin, 8C3; DLG, 4F3; and BRP, nc82) and GenScript (mouse His tag antibody and rabbit GST tag antibody).

Electrophysiology—Third instar larvae were carefully dissected as described previously (31). Two-electrode voltage clamp recordings were performed with an Axoclamp 900A amplifier (Molecular Devices, Sunnyvale, CA) using both recording (15–20 megohms) and current-passing (5–8 megohms) electrodes filled with 3 M KCl. The EJCs were recorded from ventral longitudinal muscles 6/7 in abdominal segments A2/A3 at a holding potential of −60 mV. Unless indicated otherwise, all recordings were conducted in a standard solution containing 110 mM NaCl, 5 mM KCl, 4 mM $MgCl_2$, 1.8 mM $CaCl_2$, 36 mM sucrose, and 5 mM HEPES, pH 7.0. Data were acquired using Axoclamp 900A software and Clampex 10.2 software. Synaptic currents were sampled at 10 kHz and low-pass filtered at 1 kHz. Analysis of synaptic current data was carried out in the Mini Analysis Program.

Yeast Two-hybrid Screen—The yeast two-hybrid screen was performed according to the MatchMaker™ Gold Yeast Two-Hybrid System User Manual (Clontech). Briefly, the C terminus of NRX (amino acids 1,716–1,838) was expressed as a bait in the yeast strain Y2HGold. The bait strains were incubated with prey strains Y187 that contained *Drosophila* cDNA libraries (Clontech) to generate zygotes. The zygotes then were screened on double dropout media containing X-α-Gal and aureobasidin A and further confirmed on quadruple dropout media containing X-α-Gal and aureobasidin A. The plasmids from the positive clones were sequenced and identified using the BLAST program and the FlyBase database.

Co-immunoprecipitation—Fly heads ($n = 200$) were homogenized on ice in 500 μl of PBS with a protease inhibitor containing 1% CHAPS. After 30 min of rotation at 4 °C, the extracts were centrifuged at 16,000 × *g* for 5 min at 4 °C. Next, 200 μl of the supernatant was diluted with l ml of PBS containing a protease inhibitor, after which either 20 μl of the NRX antibody or 1 μl of the preimmune serum (as a negative control) was added and incubated for 2 h at 4 °C. After blocking with 2% BSA in PBS buffer for 30 min at 4 °C, 50 μl of protein A beads (Sigma) were added to the tubes and incubated for 1 h at 4 °C. After three washes with PBS containing 0.2% CHAPS, the immune complexes were eluted with 2× SDS sample buffer and subjected to SDS-PAGE and Western blotting.

Subcellular Membrane Fraction—The subcellular membrane fractions were separated using glycerol velocity sedimentation as described previously (32). Briefly, 3 g of flies were decapitated in liquid nitrogen and ground to a powder in a mortar and pestle. The powdered heads were resuspended in 300 μl of lysis buffer (150 mM NaCl, 10 mM HEPES, pH 7.4, 1 mM EGTA) and homogenized in a Dounce pestle. The post-nuclear supernatant (10 min at 1,000 × *g*) was layered carefully onto a 5–25% glycerol gradient made in lysis buffer over a 50% sucrose cushion. The gradients were centrifuged for 1 h at 45,000 rpm in an SW60Ti rotor (Beckman, Brea, CA). All steps were performed at 4 °C. The gradient fractions then were subjected to SDS-PAGE and Western blotting.

Pulldown Assay—All GST fusion proteins, His tag proteins, and MBP fusion proteins were expressed in *Escherichia coli* BL21 cells and purified with glutathione-Sepharose (GE Healthcare, Little Chalfont, Buckinghamshire, UK), nickel-nitrilotriacetic acid-agarose (Qiagen, Hilden, Germany), and amylose resin (New England Biolabs, Ipswich, MA), respectively. To map the binding site in NRX, MBP-NSF fusion protein-coupled beads were incubated with various purified GST-NRX fragments (~20 μg of purified GST-NRX fragments each). To map the binding site in NSF, GST-NSF fusion protein-coupled beads were incubated with 40 μg of purified His-tagged C-terminal NRX fusion protein (His_6-NRX). After washing, the elution was analyzed by Western blotting.

Binding Affinity Assay—1.2 μg of GST-NSF fusion proteins were coupled to glutathione-Sepharose resins and incubated with various concentrations of purified His_6-NRX at 4 °C for overnight. For the incubations, no extra Ca^{2+} or EGTA was added. After three washes, the elution was subjected to SDS-PAGE and Western blotting.

For Ca^{2+}-dependent binding assay, GST-NRX-C-terminal fusion protein-coupled beads were incubated with the extracts of 200 fly heads (in 150 mM NaCl, 50 mM Tris-HCl, pH 7.4, containing 1% Triton X-100, and protease inhibitors) at indicated EDTA or Ca^{2+} concentrations. After washing, the elution was analyzed by Western blotting.

Immunostaining and Analysis—Immunostaining was performed as described previously (33). Briefly, third instar larvae were dissected, fixed, and then incubated with the primary antibodies, rabbit anti-NRX (1:30), rabbit anti-NSF (1:50), mouse anti-DLG (1:100), mouse anti-BRP (1:50), and goat anti-HRP (1:100) overnight. After four washes, the samples were incubated with secondary antibodies at room temperature for 2 h. After four washes, the samples were examined under an LSM 700 confocal microscope. The boutons in the ventral longitudinal muscles 6/7 of abdominal segment 3 were analyzed. To quantify the distribution of NSF, the inner circle of the DLG pattern was defined as the "presynaptic membrane." We drew a

smaller inner circle 0.25 μm away from and along the presynaptic membrane and defined the area between the two circles as the "membrane." The intensity of the membrane NSF and total NSF was measured in each genotype, and the ratio of the membrane NSF to the total NSF was quantified and presented.

Preparation of 7S SNARE Complex—7S SNARE complexes were prepared as described previously (34). Briefly, 10 flies were collected in an EP tube and frozen in liquid nitrogen and vortexed, and heads were homogenized in 50 μl of SDS sample buffer on ice. After centrifugation to the pellet cuticle, 10 μl of supernatant were loaded onto SDS-polyacrylamide gels without boiling and electrophoresed at 15 mA per gel. The gels were immunoblotted with syntaxin antibody at 1:1,000 dilution.

Statistical Analysis—Data are presented as the mean ± S.E. For all statistical analyses, two-tailed Student's *t* tests were used to compare genotypes. Significance was classified as follows: *, $p \leq 0.05$; **, $p < 0.01$; ***, $p < 0.001$; not significant (n.s.), $p > 0.05$.

Results

nrx Mutant Synapses Show Normal Short Term Synaptic Depression during Low Frequent Repetitive Nerve Stimulation—Mammals possess three *nrx* genes, each of which transcribes α- or β-*nrx*s via two promoters (35, 36). In contrast, only one α-*nrx* gene has been discovered in *Drosophila* (3, 4). To assess the potential roles of NRX in the regulation of synaptic transmission during repetitive nerve stimulation, two-electrode voltage clamp analyses were performed to record the EJCs at the *Drosophila* neuromuscular junction (NMJ). When recordings were performed at 0.5 mM Ca^{2+}, both wild-type and *nrx* mutant synapses showed mild short term synaptic depression in response to 1 Hz stimulation (Fig. 1*A*). However, the current amplitudes in *neurexin* mutant synapses were significantly reduced compared with that of wild-type synapses (Fig. 1, *A* and *B*). Previous studies in mammals have suggested that the α-NRXs functionally couple Ca^{2+} channels to the presynaptic machinery to mediate synaptic vesicle exocytosis, and studies in fly have shown that abnormal Ca^{2+} sensitivity of neurotransmitter release in *nrx* mutant synapse was completely restored when recordings were performed at 1 mM Ca^{2+} (4, 6). Consistent with a previous report (4), an increase in the Ca^{2+} concentration restored the amplitude of EJCs at the NMJ (Fig. 1, *C* and *D*). To eliminate the effects of abnormal Ca^{2+} sensitivity in neurotransmitter release, we performed our recordings at 1.8 mM Ca^{2+}. Under this condition, the *nrx* mutant synapses displayed mild short term synaptic depression in response to 1 Hz stimulation, which was similar to the response of the wild-type synapses (Fig. 1*E*). The mean current amplitudes were 154.9 ± 13.0 nA ($n = 5$) in the wild-type and 149.8 ± 15.4 nA ($n = 5$) in the *nrx* mutant synapses during the steady state (Fig. 1*F*). The steady-state quantal content in *nrx* mutant synapses was slightly reduced compared with wild-type synapses (73.8 ± 7.6 quanta *versus* 86.3 ± 7.3 quanta, Fig. 1, *G* and *H*). The initial amplitude and steady-state current amplitude therefore were indistinguishable between the wild-type and *nrx* mutant synapses in response to a 1-Hz train of stimulation (Fig. 1, *E* and *H*).

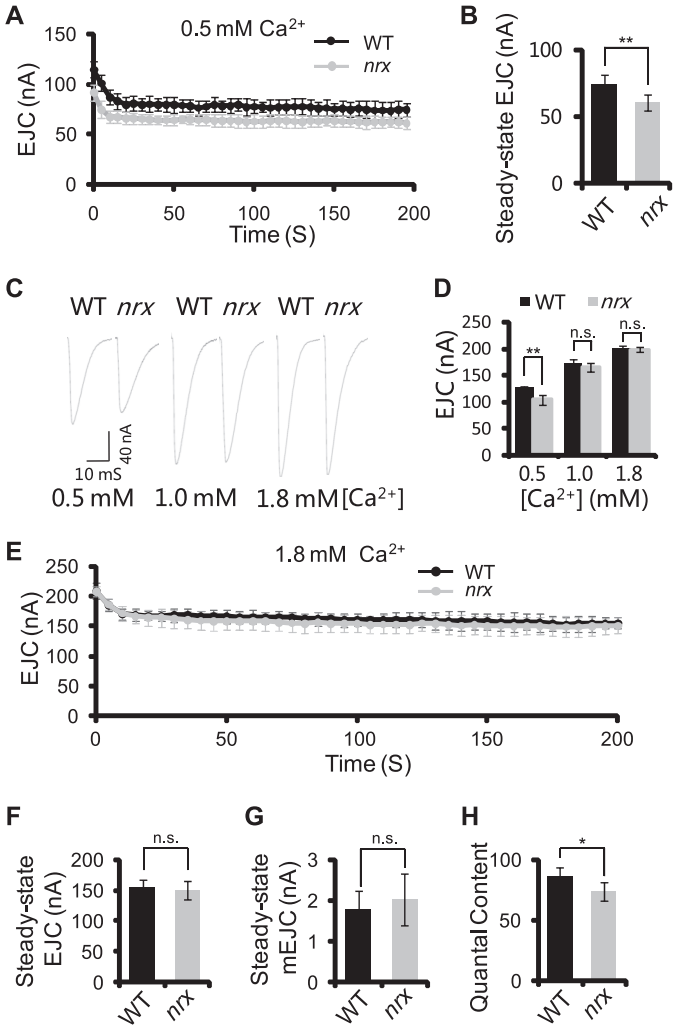

FIGURE 1. ***nrx* mutant synapses show normal synaptic depression during low frequent repetitive nerve stimulation.** *A*, 1 Hz stimulation for 200 s with 0.5 mM Ca^{2+} in wild-type (*black*, $n = 8$) and *nrx* mutant (*gray*, $n = 10$) synapses. 5 s of evoked peak EJC amplitudes are averaged at each time point and plotted as a function of time. In this and subsequent panels, the data are presented as the mean ± S.E. *B*, mean steady-state EJCs with 0.5 mM Ca^{2+} in the wild-type (*black*, $n = 8$) and *nrx* mutant (*gray*, $n = 10$) synapses. *C*, example traces of evoked EJCs supplied with variant external Ca^{2+} concentration in the wild-type and *nrx* mutant synapses. *D*, mean EJC amplitudes in the wild-type (*black*, $n = 8$) and *nrx* mutant (*gray*, $n = 8$) synapses supplied with variant external Ca^{2+} concentration. *E*, 1 Hz stimulation for 200 s with 1.8 mM Ca^{2+} in wild-type (*black*, $n = 5$) and *nrx* mutant (*gray*, $n = 5$) synapses. *F*, mean steady-state EJCs with 1.8 mM Ca^{2+} in the wild-type (*black*, $n = 5$) and *nrx* mutant (*gray*, $n = 5$) synapses. *G*, mean steady-state miniature EJCs with 1.8 mM Ca^{2+} in the wild-type (*black*, $n = 898$) and *nrx* mutant (*gray*, $n = 701$) synapses. *H*, mean steady-state quantal content with 1.8 mM Ca^{2+} in the wild-type (*black*, $n = 5$) and *nrx* mutant (*gray*, $n = 5$) synapses.

nrx Mutant Synapses Exhibit Rapid Short Term Synaptic Depression during Tetanic Nerve Stimulation—We further performed two-electrode voltage clamp recordings to examine the EJCs at the *Drosophila* NMJ upon 40 Hz tetanic nerve stimulation. Interestingly, a marked activity-dependent reduction in the amplitude of the evoked currents was observed in the *nrx* mutant relative to the wild-type synapses under 0.5 mM Ca^{2+} conditions (Fig. 2, *A* and *B*). Rapid short term synaptic depression in *nrx* mutant synapses might be due to abnormal Ca^{2+} sensitivity and/or some other potential effectors. To eliminate the effects of abnormal Ca^{2+} sensitivity in short term synaptic

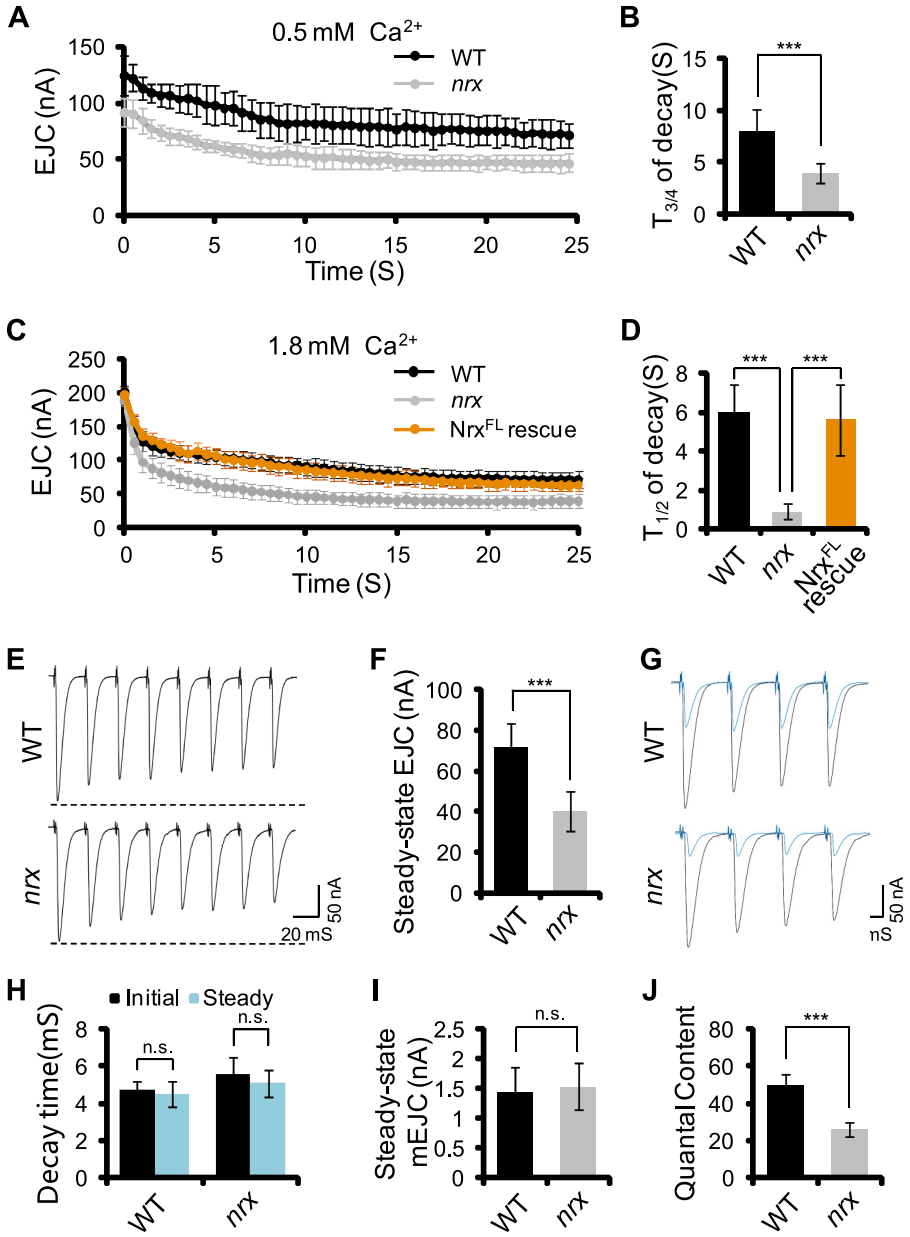

FIGURE 2. ***nrx* mutant synapses show rapid synaptic depression during tetanic nerve stimulation.** *A,* 40 Hz stimulation for 25 s with 0.5 mM Ca^{2+} in wild-type (*black, n* = 8) and *nrx* mutant (*gray, n* = 10) synapses. 0.5 s of evoked peak EJC amplitudes are averaged at each time point and plotted as a function of time. *B,* quantification of the time for EJC amplitudes declining to 75% in each genotype synapses. *C,* 40 Hz stimulation for 25 s in wild-type (*black, n* = 10), *nrx* mutant (*gray, n* = 8), and full-length NRX rescue (*orange, n* = 8) synapses. The rescue of NRX is conducted in *Ok6-GAL4/+;UAS-*NRX, $nrx^{\Delta 83}/nrx^{273}$. 0.5 s of evoked peak EJC amplitudes are averaged at each time point and plotted as a function of time. *D,* quantification of the time for EJCs declining to 50% of the initial amplitude in each genotype. *E,* example traces of first eight evoked EJCs in the wild-type (*upper trace*) and *nrx* mutant synapses (*lower trace*) during 40 Hz stimulation. *F,* The mean steady-state EJCs in the wild-type (*black, n* = 10) and *nrx* mutant (*gray, n* = 8) synapses. *G,* example traces of evoked EJCs in the wild-type (*upper trace*) and *nrx* mutant (*lower trace*) synapses during tetanic nerve stimulation. *Black traces* represent four EJCs at initial state and *blue traces* show four EJCs at steady state. *H,* decay time of EJCs at the initial state and the steady state in each genotype. The decay time were determined by averaging 10 EJCs in each state. *I,* mean steady-state miniature EJCs in the wild-type (*black, n* = 824) and *nrx* mutant (*gray, n* = 960) synapses. *J,* mean steady-state quantal content in wild-type (*black, n* = 10) and *nrx* (*gray, n* = 8) synapses.

depression, we further conducted the recordings at 1.8 mM Ca^{2+}. Under this condition, *nrx* mutant synapses still exhibit a rapid synaptic depression compared with wild-type synapses (Fig. 2, *C* and *D*). The amplitude of the evoked currents in the wild-type synapses quickly declined to ~75% of the initial stimulus after eight stimuli (Fig. 2*E*) and to 50% after 6.0 ± 1.5 s and then slowly reached a steady state of 72.0 ± 11.6 nA (n = 10) after ~20 s (Fig. 2, *C–F*). In contrast, the amplitude of the evoked currents in the *nrx* mutant synapses dropped precipitously to ~62% of the initial stimulus after eight stimuli (Fig. 2*E*) and to 50% after 0.9 ± 0.4 s and reached a steady state of 40.5 ± 9.9 nA (n = 8) after ~15 s (Fig. 2, *C–F*). The rapid short term synaptic depression in the *nrx* mutant synapse is caused by the presynaptic loss of NRX, as the neural expression of NRX restored this deficit in the *nrx* mutant synapses (Fig. 2, *C* and *D*).

Short term synaptic depression during tetanic stimulation in the *nrx* mutant synapses may reflect either the rapid desensitization of postsynaptic glutamate receptors or deficits in synap-

tic vesicle release (31, 37). To differentiate between these two possibilities, we compared the kinetics of the individual synaptic currents at the initiate state and at the steady state of tetanic stimulation. In both wild-type and *nrx* mutant synapses, the decay time of the individual synaptic currents at the steady state were comparable with that at the initiate state of tetanic stimulation (Fig. 2, *G* and *H*). These observations imply that the rapid current decline in the *nrx* mutant synapses during tetanus is not due to the desensitization of postsynaptic glutamate receptors.

Next, we compared the rate of synaptic vesicle release in wild-type and *nrx* mutant synapses. To determine the quantal content of the nerve-evoked synaptic currents at the steady state, we measured the evoked currents and the spontaneous miniature currents at the steady state. The mean of evoked current was 72.0 ± 11.6 ($n = 10$) in the wild-type synapses and 40.5 ± 9.9 ($n = 8$) in the *nrx* mutant synapses (Fig. 2*F*). The averaged miniature current was 1.45 ± 0.42 ($n = 824$) in the wild-type synapses and 1.54 ± 0.40 ($n = 960$) in the *nrx* mutant synapses (Fig. 2*I*). Thus, the steady-state quantal content was 49.8 ± 8.0 quanta ($n = 10$) in the wild-type synapses compared with 26.2 ± 9.9 quanta ($n = 8$) in the *nrx* mutant synapses (Fig. 2*J*). This result indicates that synaptic vesicle release is impaired in the *nrx* mutant synapses during tetanic stimulation.

Intracellular Region of NRX Regulates Synaptic Vesicle Release—NRX is a cell adhesion molecule that contains a single transmembrane domain. Given that the synaptic vesicle release machinery operates in the cytosolic region of the presynaptic terminals (38), we questioned whether the intracellular region of NRX is required for synaptic vesicle release during tetanic stimulation. To test this possibility, we generated a C-terminally truncated NRX transgene $p(UAS\text{-}NRX^{\Delta C})$ in which the intracellular region of NRX was deleted and expressed this transgene in motor neurons. Previous studies have shown that the polarized targeting of NRX to synapses is regulated by their C-terminal sequences (39, 40). To examine whether $NRX^{\Delta C}$ is able to distribute into the presynaptic terminals of NMJs, we performed the antibody staining analysis. The results showed that full-length NRX was successfully distributed into the presynaptic terminals (Fig. 3, *A* and *B*). Consistent with previous findings, lack of the intracellular region of NRX led to massive $NRX^{\Delta C}$ retained in the motor neuron axons (Fig. 3, *A* and *B*). However, we found that a portion of $NRX^{\Delta C}$ was successfully distributed into the presynaptic terminals (Fig. 3, *A* and *B*). Meanwhile, the amount of $NRX^{\Delta C}$ distributed into the presynaptic terminals was comparable with that of full-length NRX (Fig. 3, *A* and *B*).

Because the truncated NRX was successfully distributed into the presynaptic terminals, we therefore performed the rescue experiments by using these transgenes. The synaptic current recording at the NMJ with 1.8 mM Ca^{2+} showed that the expression of $NRX^{\Delta C}$ failed to restore the defective short term synaptic depression in the *nrx* mutant synapses (Fig. 3, *C–E*), which indicates that the intracellular region of NRX is essential for synaptic vesicle release during tetanic stimulation. The PDZ-binding motif in the NRX molecule is able to associate with several molecules involved in the synaptic vesicle exocytosis machinery, including synaptotagmin and the PDZ domain-containing proteins CASK and Mints (16–18). To investigate the potential role of the PDZ-binding motif in the regulation of short term synaptic depression, we generated a NRX transgene with a deleted PDZ-binding motif ($NRX^{\Delta 4}$) and performed the rescue experiments. Interestingly, the expression of $NRX^{\Delta 4}$ failed to restore the rapid current decline in the first several dozen stimulations but recovered the reduced mean EJCs and quantal content at the steady state (Fig. 3, *C–G*). These observations strongly suggest that other intracellular regions of NRX also regulate synaptic vesicle release.

To examine the role of the cytoplasmic tail in synaptic vesicle release under normal conditions, we also recorded these rescue synapses under 0.5 mM Ca^{2+} conditions. Interestingly, expression of all NRX transgenes successfully restored the initial current amplitudes (Fig. 4, *A–C*), indicating the extracellular region of NRX is sufficient for coupling Ca^{2+} channels. These observations are supported by the previous study, which shows that extracellular domains of NRX participate in regulating synaptic transmission (41). Consistent with the recordings performed in 1.8 mM Ca^{2+} conditions, expression of full-length NRX and $NRX^{\Delta 4}$, but not $NRX^{\Delta C}$, restored the reduced mean EJCs at the steady state (Fig. 4*D*). These results indicate that other intracellular regions of NRX regulate synaptic vesicle release at normal conditions.

NRX Associates with NSF in Vivo—To determine the molecular mechanism by which NRX regulates synaptic vesicle release during tetanic stimulation, we performed a yeast two-hybrid screen of a *Drosophila* cDNA library using the intracellular region of the *Drosophila* homolog of α-NRX as the bait. We identified several previously unreported binding proteins (Table 1), including NSF that mediates SNARE complex disassembly and plays an important role in synaptic vesicle release (Fig. 5*A*) (42, 43). To evaluate the NRX/NSF interaction *in vivo*, we conducted a subcellular distribution analysis and co-immunoprecipitation assays. We separated the plasma membrane and synaptic vesicle membrane by sedimentation in a glycerol gradient (32). Quantitative Western blotting revealed that NRX existed predominantly in the plasma membrane-containing fractions where the plasma membrane marker Na^+/K^+-ATPase-α was present (Fig. 5*B*). Meanwhile, although NSF was present in both the plasma membrane-containing and non-plasma membrane-containing fractions, more than 50% of the NSF was in the plasma membrane-containing fractions (Fig. 5*B*). The co-immunoprecipitation experiment further demonstrated that NRX interacted with NSF *in vivo* (Fig. 4*C*). These results demonstrate that NRX associates with NSF at the presynaptic terminals.

In addition, we also measured the NSF-binding capacity of NRX with a pulldown assay. The results from this assay revealed that NRX bound to NSF in a concentration-dependent and saturable manner ($K_d = 4.4\ \mu M$) (Fig. 5*D*). Furthermore, we examined the NSF-binding capacity of NRX in the fly head extracts with different Ca^{2+} concentrations. Interestingly, NRX showed the highest binding capacity with NSF in 0.5 mM Ca^{2+} condition and exhibited the declined binding ability with the increasing of Ca^{2+} concentration (Fig. 5*E*). These data indicate that the NSF-binding capacity of NRX is modulated by Ca^{2+} concentration.

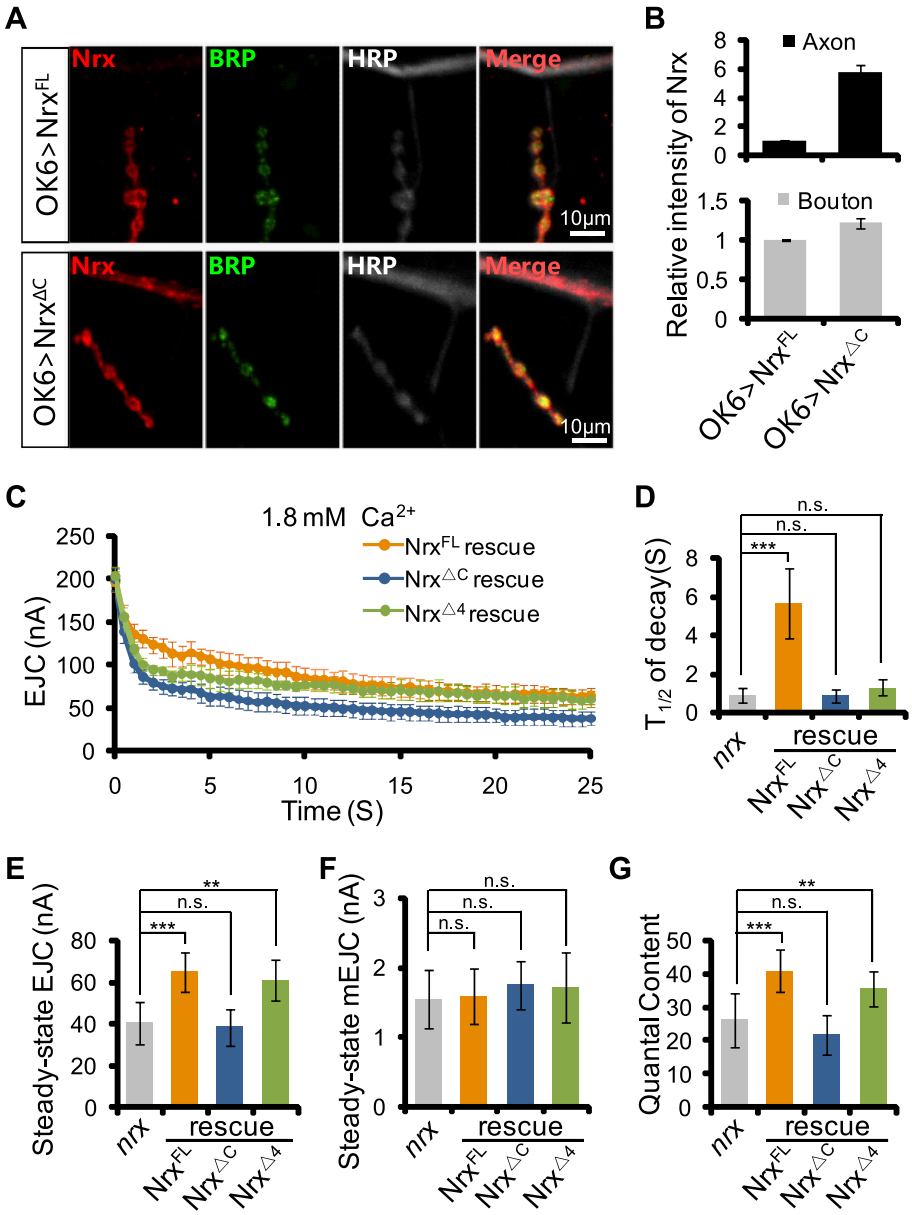

FIGURE 3. **Intracellular region of NRX regulates synaptic vesicle release at 1.8 mM Ca^{2+} condition.** *A*, immunostaining images indicating both full-length NRX and C-terminally truncated NRX are able to distribute into the presynaptic terminals of NMJs. *B*, quantification of relative mean fluorescence intensity of NRX in axons and boutons. *C*, 40 Hz stimulation for 25 s with 1.8 mM Ca^{2+} in indicated rescue synapses. The rescue of NRX was conducted in *UAS*-$NRX^{\Delta C}$; *Ok6-GAL4/+*; $nrx^{\Delta 83}/nrx^{273}$ (*blue*, $n = 7$), and *Ok6-GAL4/+*;*UAS*-$NRX^{\Delta 4}$, $nrx^{\Delta 83}/nrx^{273}$ (*green*, $n = 6$). 0.5 s of evoked peak EJC amplitudes are averaged at each time point and plotted as a function of time. *D*, quantification of the time for EJCs declining to 50% of the initial amplitude in indicated genotype flies. *E–G*, quantification of the steady-state EJC amplitudes, miniature EJC amplitudes, and quantal content in each genotype synapse.

NRX Binds to the D2 Domain of NSF—The intracellular region of NRX contains 122 amino acids, including a functional PDZ-binding motif (Fig. 6*A*) (3). We investigated which part within the intracellular region that mediates the interaction with NSF. The pulldown assay revealed that the purified NSF protein was able to bind with the fragments NRX(1730–1837), NRX(1730–1813), and NRX(1730–1833) but not with the fragments NRX(1730–1759) and NRX(1730–1787) (Fig. 6*A*). These observations indicate that amino acids 1788–1813 in the intracellular region of NRX mediate the interaction with NSF. To further validate the NSF-binding sites in NRX, we expressed and purified the mutant NRX(Δ1788–1813) that deleted amino acids 1788–1813 of NRX. The pulldown assay revealed that NSF protein failed to bind with NRX(Δ1788–1813) (Fig. 6*B*). An alignment analysis revealed that several amino acids are conserved in this region across different species (Fig. 6*C*), which suggests that the NRX/NSF interaction may occur in other species.

NSF has three distinct domains as follows: two homologous D domains (D1 and D2) and an N domain (Fig. 6*D*) (38). To determine which domain within the NSF protein interacts with NRX, pulldown assays using several constructs encoding truncated NSF fragments fused to GST were performed (Fig. 6*D*). The results revealed that purified NRX is able to bind to the full-length NSF protein (NSF(1–745)) as well as the truncated fragment NSF(1–588) but not the truncated fragments NSF(1–

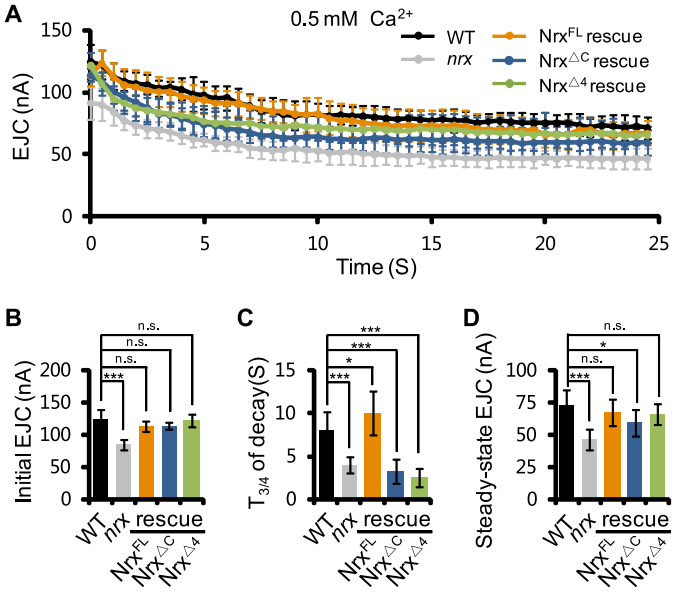

FIGURE 4. **Intracellular region of NRX regulates synaptic vesicle release at 0. 5 mM Ca^{2+} condition.** *A*, 40 Hz stimulation for 25 s with 0.5 mM Ca^{2+} in wild-type (*black*, $n = 8$), *nrx* mutant (*gray*, $n = 10$), and three indicated rescue (*orange*, $n = 8$; *blue*, $n = 7$; *green*, $n = 8$) synapses. 0.5 s of evoked peak EJC amplitudes are averaged at each time point and plotted as a function of time. *B–D*, quantification of the initial EJC amplitudes, the time for EJC amplitudes declining to 75%, and the steady-state EJC amplitudes in each genotype synapses.

TABLE 1

Yeast two-hybrid screening identify some proteins interacted with the intracellular region of NRX

Clone	Genes	Sequences	Molecular functions
		amino acids	
54	*tpnc4*	1–152	Calcium ion binding
73	*fkbp59*	157–440	Peptidylprolyl cis-trans isomerase activity
88	*CG33978-PC*	2,065–2,289	Calcium ion binding
XF5	*CG33978-PC*	2,107–2,289	Same as above
XH4	*CG33978-PC*	2,090–2,289	Same as above
92	*CG9238*	176–331	Protein phosphatase 1 binding
146	*nrv3*	37–247	Sodium:potassium-exchanging ATPase activity
174	*tbcb*	1–244	Unknown
YK2	*tbcb*	1–244	Unknown
176	*mbf1-PC*	1–188	Transcription co-activator activity
184	*CKiiα-I3-PA*	1–280	Protein kinase activity
G8	*cKiiα-I3-PA*	1–181	Same as above
E10	*ephrin*	605–652	Ephrin receptor binding
F4	*CG17360*	518–833	Unknown
G5	*rfabg*	364–493	Lipid transporter activity; retinol binding
K1	*rfabg*	464–623	Same as above
L3	*CG15576*	1–123	Unknown
M6	*CG12374*	335–422	Metallocarboxypeptidase activity
XB9	*CG33123*	1,102–1,182	Aminoacyl-tRNA editing activity
XN7	*vtd*	482–715	Chromatin binding
YH1	*comt*	351–745	ATPase activity
YJ4	*med26*	1,216–1,546	Transcription factor activity
YL7	*CG7102*	364–621	Unknown

513), NSF(1–389), or NSF(1–175) (Fig. 6*D*). These results suggest that the amino acid sequence 514–588 in the NSF protein is a critical component of the NRX interaction with NSF. An alignment analysis revealed that this region of NSF (Fig. 6*E*), which is partially within the D2 domain essential for the hexamerization of NSF (44, 45), is highly conserved across species.

NRX/NSF Interaction Is Essential for NSF Recruitment—To determine the potential role of the NRX/NSF interaction in the regulation of NSF function and subsequent synaptic vesicle release, we examined the distribution of NSF in *nrx* mutant synapses. The distribution of NSF was determined relative to the markers for the postsynaptic membrane as well as active zone regions of synapse where synaptic vesicles dock and fuse. In the wild-type NMJs, the NSF occupied the cytosolic regions within the presynaptic boutons and existed predominantly near the presynaptic membrane in a similar ratio to the postsynaptic marker DLG (Fig. 7, *A–C*). In contrast, in the *nrx* mutant NMJs, a large portion of the NSF fell into the cytosolic region within the boutons (Fig. 7, *A–C*). To validate the distribution of NSF within the wild-type and *nrx* mutant synapses, the plasma and synaptic vesicle membranes were separated by sedimentation in a glycerol gradient. Quantitative Western blotting revealed that the sedimentation profile of NSF was shifted significantly from the plasma membrane fractions to the cytosolic fractions in the *nrx* mutant synapses compared with the wild-type synapses (Fig. 7*D*). These findings indicate that the loss of NRX results in an altered NSF distribution at the presynaptic terminals.

To address whether the NRX/NSF interaction facilitates the recruitment of NSF to the presynaptic terminals, we performed rescue experiments. Interestingly, the expression of the full-length NRX transgene *p*(*UAS-NRX*) but not the C-terminally truncated Neurexin transgene *p*(*UAS-NRX*$^{\Delta C}$) rescued the abnormal NSF distribution in the *nrx* mutant synapses (Fig. 7, *E* and *F*). These observations strongly suggest that the NRX/NSF interaction is essential for the recruitment of NSF to the presynaptic terminals.

NSF is known to mediate SNARE complex disassembly (42, 43). A biochemical analysis has shown that SDS-resistant 7S SNARE complexes accumulate in *comt* mutant flies following the disruption of NSF activity (43). We therefore asked whether the loss of the NRX/NSF interaction would affect SNARE complex disassembly. Western blotting analysis revealed that SDS-resistant 7S SNARE complex was accumulated in *nrx* mutants compared with wild-type flies (Fig. 7, *G* and *H*). These data suggest that the NRX/NSF interaction promotes SNARE complex disassembly and the subsequent synaptic vesicle release during tetanic stimulation.

Taken together, these data support a model in which NRX/NSF interaction facilitates the recruitment of NSF in the presynaptic terminals and restricts the movement of NSF at rest conditions. With the increase of terminal Ca^{2+} concentration during stimulation, NRX releases NSF to facilitate the disassembly of SNARE complexes.

Discussion

NRX Facilitates Repetitive Synaptic Vesicle Release—Previous studies have shown that the α-NRXs functionally couple Ca^{2+} channels to the presynaptic machinery to mediate synaptic vesicle exocytosis (4, 6) and that defective synaptic vesicle release can be restored with 1 mM Ca^{2+} (4). In our experiments, 1.8 mM Ca^{2+} was used to eliminate the effects of abnormal Ca^{2+} sensitivity in neurotransmitter release. Under this condition, we showed that *nrx* mutant synapses exhibit rapid short term synaptic depression and reduced quantal content of nerve-evoked synaptic currents at the steady state during tetanic stimulation. These observations suggest that NRX regulates activity-dependent synaptic plasticity. Similar observations have been reported in the fast-twitch diaphragm muscle of the

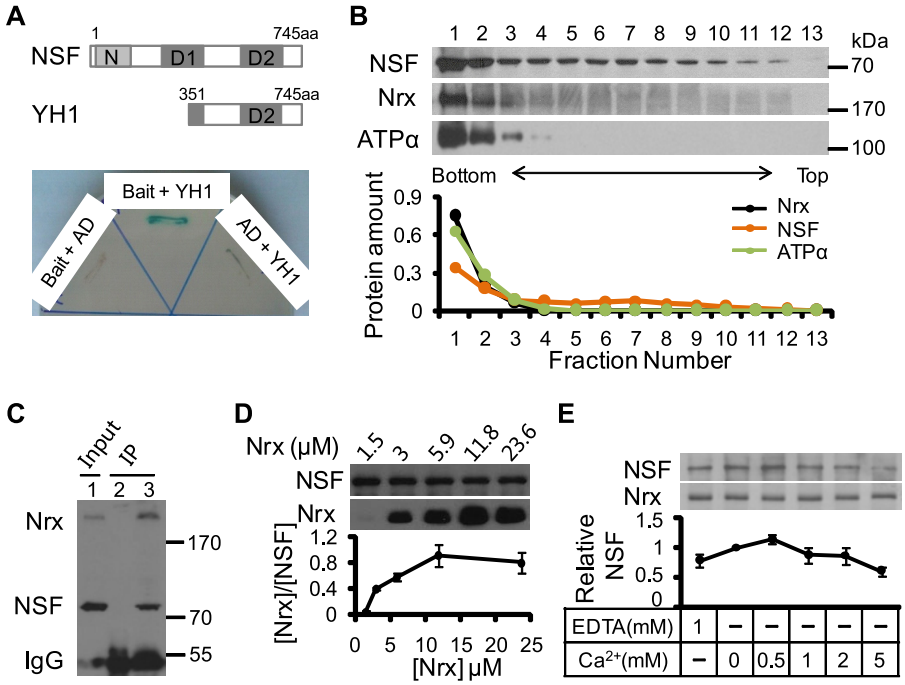

FIGURE 5. **NRX interacts with NSF.** *A,* yeast two-hybrid screen identified one cDNA of NSF, YH1, that interacts with the intracellular region of NRX. The NSF protein structure and the encoded region of YH1 are shown in the *left panel*. AD, pGADT$_7$-RecAB. *aa,* amino acids. *B,* immunoblots of fractions from a postnuclear membrane density gradient display the distribution of NRX and NSF. The *top* and *bottom* of the gradient are indicated. Na^+/K^+-ATPase-α is used to indicate plasma membrane-enriched fractions. The sedimentation profiles of each protein are plotted in the *lower panel*. *C,* fly head extracts were immunoprecipitated with either the preimmune serum (*lane 2*) or the anti-NRX antiserum (*lane 3*). The results show that NRX co-immunoprecipitates with NSF *in vivo*. *D,* GST-NSF fusion proteins were coupled to glutathione-agarose resin and incubated with various concentrations of the purified His$_6$-NRX fusion protein to measure the binding affinity of NRX/NSF. The binding proteins were eluted and analyzed by Western blotting analysis. The ratios of His$_6$-NRX to GST-NSF were calculated from three independent experiments, and plotted as the concentration of His$_6$-NRX. *E,* GST-NRX C-terminal fusion protein-coupled beads were incubated with fly head extracts at indicated EDTA or Ca^{2+} concentrations. The relative NSF amount was plotted ($n = 3$).

α-NRX double knock-out mouse, which indicates that presynaptic efficacy but not presynaptic homeostatic plasticity is normal under basal conditions (46).

Deficits in both the presynaptic neurotransmitter release machinery and the postsynaptic neurotransmitter receptors may cause rapid short term synaptic depression (31, 37). As a presynaptic adhesion molecule, NRX interacts with the postsynaptic adhesion molecule, Neuroligin, and bridges the synaptic cleft that aligns the presynaptic neurotransmitter release machinery with the postsynaptic neurotransmitter receptors. It has been suggested that the activity-dependent regulation of the NRX/Neuroligin interaction mediates learning-related synaptic remodeling and long term facilitation (47). A recent study reveals that the alternative splicing of presynaptic NRX-3 controls postsynaptic AMPA receptor trafficking and long term plasticity in mice (48). In this study, we showed that the kinetics of the individual synaptic currents were stable during tetanic stimulation in the *nrx* mutant synapses. Moreover, we showed that NRX mediated synaptic plasticity through the presynaptic machinery, which was supported by our rescue experiments.

NRX Interacts with NSF—The intracellular sequence of NRX, including the C-terminal PDZ-binding motif, is identical across several vertebrate and invertebrate species. Mammalian NRXs only possesses a short cytoplasmic tail (55 amino acids), including a PDZ-binding motif (36). To identify the potential binding partners, several laboratories have conducted yeast two-hybrid screening by using the cytosolic tail of mammalian NRX as a bait. Two PDZ-containing proteins, CASK and syntenin, have been identified in the previous screening (17, 19), and further studies show that the binding between CASK and NRX is abolished by deletion of the last three amino acids of the intracellular C-terminal region of NRX (17). However, it seems that the previous screenings are not saturated, as the NRX-interacted protein Mints was not identified in these screenings (18).

Drosophila NRX contains a long cytoplasmic tail (122 amino acids), including a functional PDZ-binding motif (3). Thus, it is possible that the long cytoplasmic tail may associate with some partners in a PDZ-independent manner. In this study, normalized *Drosophila* cDNA libraries were used in our screening, which helps to identify the binding partner with low abundance. In our screening, 23 cDNAs clones that encode the fragments of 18 proteins were recovered. Our previous study has demonstrated that the cytoplasmic tail of NRX associates with RFABG and facilitates the retinol transport (29). In this study, we identified the intracellular region of NRX binds with NSF through the amino acid sequence 1788–1813 but not the PDZ-binding motif of NRX. We found that this NRX/NSF interaction is essential for the NSF recruitment to the presynaptic terminals and plays an important role in synaptic vesicle release. In addition, we provided multiple lines of evidence that NRX associates with NSF at the presynaptic terminals. An alignment analysis of the NSF-binding site of NRX revealed that this sequence is conserved across different species. Moreover, this sequence is present across many proteins that serve different functions, which implies that this sequence may be essential for protein interactions.

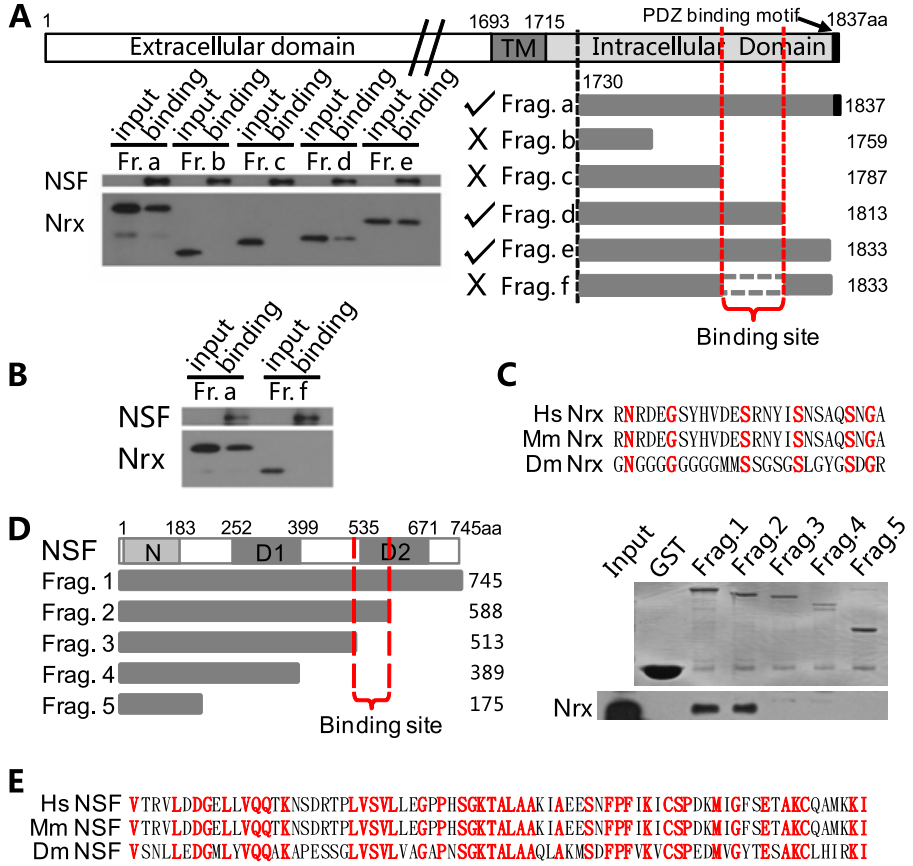

FIGURE 6. **Mapping the NRX/NSF-binding sites in each molecule.** *A* and *B*, pulldown assay mapped residues 1,788–1,813 (*bracket*) as an NSF-binding site of NRX. The MBP-NSF fusion proteins were coupled to amylase resin for the pulldown assay. The pulldown samples as well as a portion (5% of the input for pulldown) of the purified GST-fused NRX fragments were loaded for Western blotting. *Fr.*, fraction; *aa*, amino acid. *C*, sequence alignment of the NSF-binding site of NRX shows conserved amino acids across species (in *red*). *Hs, Homo sapiens*; *Mm, Mus musculus*; and *Dm, Drosophila melanogaster*. *D*, pulldown assay mapped residues 514–588 (*bracket*) as an NRX-binding site of NSF. Various GST-fused NSF fragments (*Frag.*) were coupled to glutathione-agarose resin and incubated with the purified His_6-NRX fusion protein. *Left*, encoded regions of the NSF fragments. *Right upper panel*, Coomassie Blue staining of GST-fused NSF fragments. *Right lower panel*, Western blots of the pulldown assays. The pulldown samples as well as a portion (10% of the input for the pulldown) of the purified His_6-NRX fusion proteins were loaded for Western blotting. *E*, sequence alignment of the NRX-binding site of NSF shows conserved amino acids across species (in *red*). *Hs, H. sapiens*; *Mm, M. musculus*; and *Dm, D. melanogaster*.

Each NSF molecule contains an N-terminal domain that is responsible for the interaction with α-SNAP and the SNARE complex, a low affinity ATP-binding domain (D1 domain) whose hydrolytic activity is associated with NSF-driven SNARE complex disassembly and a C terminal high affinity ATP-binding domain (D2 domain) (44, 45, 50, 51). In this study, we mapped the NRX-binding sites of NSF to the D2 domain, which mediates the ATP-dependent oligomerization of NSF (45, 52). An alignment analysis showed that both the D2 domain in NSF and the NSF-binding site in NRX are highly conserved. This result suggests that the NRX/NSF interaction may occur in other species, a possibility that needs to be investigated further.

It has been documented that the D2 domain of NSF is essential for its hexamerization (44, 45). In this study, we show that NRX exhibits a declined NSF binding capacity in high Ca^{2+} concentration. These observations suggest that NSF can be released from NRX under stimulation. Although NRX and NSF do not bind with Ca^{2+} directly, it is possible that they undergo Ca^{2+} signaling-dependent modifications or bind with some Ca^{2+}-binding proteins. In our yeast two-hybrid screening, one potential Ca^{2+}-binding protein (CG33978) has been identified. However, the mechanism of how NRX releases NSF under high Ca^{2+} concentration need to be further investigated.

NRX/NSF Interaction Regulates Activity-dependent Short Term Synaptic Depression—Previous studies have shown that the PDZ-binding motif of NRX associates with several molecules involved in the synaptic vesicle exocytosis machinery, including synaptotagmin and the PDZ domain-containing proteins CASK and Mints (16–18). Synaptotagmin functions as a Ca^{2+} sensor and controls synaptic membrane fusion machinery (26). Adaptor protein Mints regulates presynaptic vesicle release (53), whereas the other adaptor protein CASK is not essential for the Ca^{2+}-triggered presynaptic release (54). In contrast, CASK interacts with NRX and protein 4.1 to form a trimeric complex and regulates synapse formation (55, 56). The process of synaptic vesicle release includes several consecutive steps, docking, priming, and fusion (26). Depending on the stimulation given to synapses, different synaptic vesicle trafficking steps become rate-limiting for synaptic vesicle release. This causes short term changes in synaptic transmission that determine many higher brain functions such as sound localization, sensory adaptation, or even working memory (57). Thus, the PDZ-binding motif-linked synaptic vesicle exocytotic machinery might regulate the different steps during synaptic vesicle release. Indeed, *nrx* mutant synapses that express $NRX^{\Delta 4}$ exhibit a rapid current decline over the first several

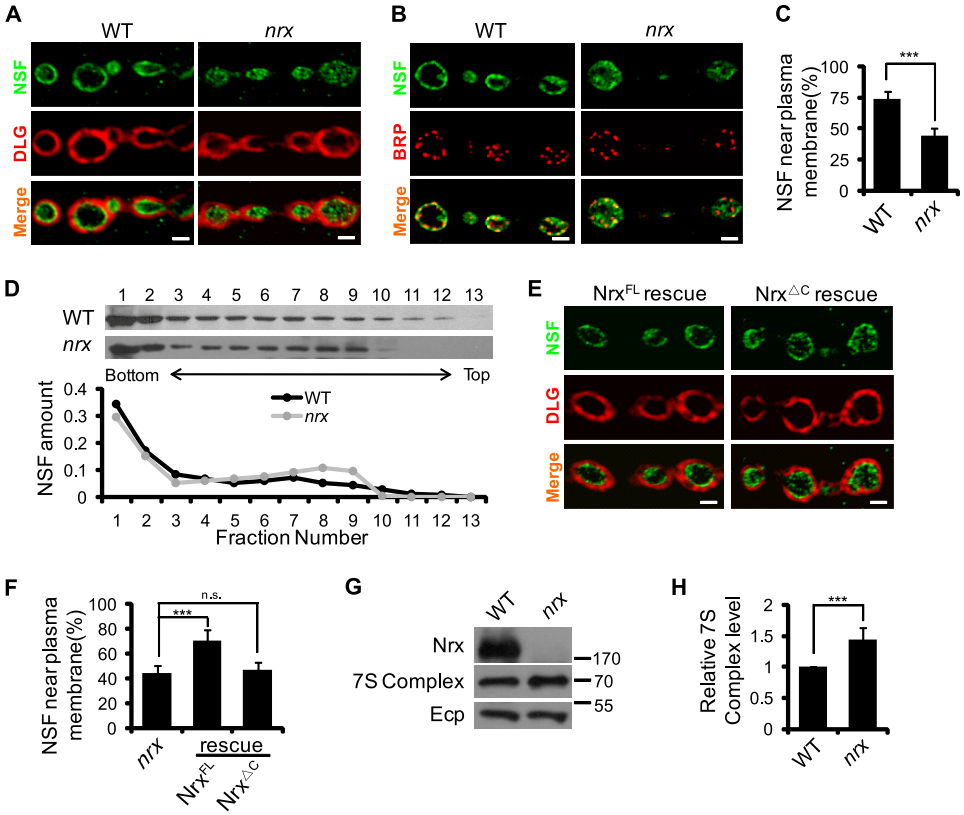

FIGURE 7. **NRX/NSF interaction recruits NSF and promotes SNARE complex disassembly.** *A* and *B*, distribution of NSF in the NMJs of each genotype was analyzed in the ventral longitudinal muscles 6/7 of abdominal segment 3. *C*, quantification of the NSF distribution in wild-type and *nrx* mutant NMJs. For each genotype, six muscles 6/7 of abdominal segment 3 from six larvae were examined. *D*, immunoblots of the fractions from the postnuclear membrane density gradient from wild-type and *nrx* mutant flies are presented in the *upper panel*. The *top* and *bottom* of the gradients are indicated. The sedimentation profiles of each protein are plotted in the *lower panel*. *E*, immunostaining of NSF in the rescue NMJs. *F*, quantification of NSF distribution in the rescue NMJs. *G*, Western blotting shows the amount of 7S complexes in wild-type or *nrx* mutants. *Drosophila* Ecp was used for loading control. *H*, quantification of the relative 7S complex amount in each genotype.

dozen stimulations. In contrast, the expression of $NRX^{\Delta 4}$ largely restores the reduced steady-state mean EJCs and quantal content in *neurexin* mutant synapses. Together with the C-terminally truncated NRX rescue experiments, these data suggest that intracellular regions of NRX other than the PDZ-binding motif also regulate short term synaptic depression. The existing literature extensively documents the roles of NSF in SNARE complex disassembly and short term synaptic depression (38, 43, 58). In this study, we extended these findings to show that the NRX/NSF interaction facilitates the recruitment of NSF to the presynaptic terminals and promotes the subsequent SNARE complex disassembly.

Previous studies have established that the NSF hexamer serves as the only active form for SNARE complex disassembly (23, 45, 49, 50, 59). In this study, our binding assay showed that purified NRX binds to NSF in a concentration-dependent and saturable manner. NRXs appear to serve as scaffold proteins to recruit NSF, and the NRX/NSF interaction may promote SNARE complex disassembly *in vivo*. Live image studies have shown that NSF mutant (*i.e. comt*) synapses exhibit defective NSF re-distribution during tetanic nerve stimulation (28). In this study, immunocytochemical and sedimentation analyses revealed that a lack of the NRX/NSF interaction results in an altered distribution of NSF and an accumulation of 7S SNARE complexes. Our results imply that NRX/NSF interaction serves as a potential mechanism to restrict the mobilization of NSF.

Our electrophysiological recordings revealed that synaptic depression was comparable between *nrx* mutant synapses and wild-type synapses in response to low frequency stimulations. The long intervals between low frequency stimulations may allow the remaining NSF to disassemble the SNARE complexes and generate enough free t-SNARE for the subsequent synaptic vesicle fusion events. Another possibility that needs to be investigated further is that tetanic stimulation may have other effects on the re-distribution of NSF.

In summary, our study provides evidence that the NRX/NSF interaction recruits NSF to the presynaptic terminals and promotes SNARE complex disassembly. Our findings have revealed a previously unknown role of NRX in the regulation of neurotransmitter release and provide a linkage between the presynaptic adhesion molecules and the presynaptic plasticity machinery.

Acknowledgments—We thank Dr. Manzoor A. Bhat for providing the nrx^{273} flies, and Dr. Zhengping Jia, Dr. Wei Lu, Dr. Zikai Zhou, and members of the Han laboratory for their critical comments on the manuscript.

References

1. Scheiffele, P. (2003) Cell-cell signaling during synapse formation in the CNS. *Annu. Rev. Neurosci.* **26,** 485–508

2. Dean, C., Scholl, F. G., Choih, J., DeMaria, S., Berger, J., Isacoff, E., and Scheiffele, P. (2003) Neurexin mediates the assembly of presynaptic terminals. *Nat. Neurosci.* **6,** 708–716
3. Zeng, X., Sun, M., Liu, L., Chen, F., Wei, L., and Xie, W. (2007) Neurexin-1 is required for synapse formation and larvae associative learning in *Drosophila*. *FEBS Lett.* **581,** 2509–2516
4. Li, J., Ashley, J., Budnik, V., and Bhat, M. A. (2007) Crucial role of *Drosophila* neurexin in proper active zone apposition to postsynaptic densities, synaptic growth, and synaptic transmission. *Neuron* **55,** 741–755
5. Yamagata, M., Sanes, J. R., and Weiner, J. A. (2003) Synaptic adhesion molecules. *Curr. Opin. Cell Biol.* **15,** 621–632
6. Missler, M., Zhang, W., Rohlmann, A., Kattenstroth, G., Hammer, R. E., Gottmann, K., and Südhof, T. C. (2003) α-Neurexins couple Ca^{2+} channels to synaptic vesicle exocytosis. *Nature* **423,** 939–948
7. Ichtchenko, K., Hata, Y., Nguyen, T., Ullrich, B., Missler, M., Moomaw, C., and Südhof, T. C. (1995) Neuroligin 1: a splice site-specific ligand for β-neurexins. *Cell* **81,** 435–443
8. Boucard, A. A., Chubykin, A. A., Comoletti, D., Taylor, P., and Südhof, T. C. (2005) A splice code for trans-synaptic cell adhesion mediated by binding of neuroligin 1 to α- and β-neurexins. *Neuron* **48,** 229–236
9. Sugita, S., Saito, F., Tang, J., Satz, J., Campbell, K., and Südhof, T. C. (2001) A stoichiometric complex of neurexins and dystroglycan in brain. *J. Cell Biol.* **154,** 435–445
10. Missler, M., Hammer, R. E., and Südhof, T. C. (1998) Neurexophilin binding to α-neurexins. A single LNS domain functions as an independently folding ligand-binding unit. *J. Biol. Chem.* **273,** 34716–34723
11. Missler, M., and Südhof, T. C. (1998) Neurexophilins form a conserved family of neuropeptide-like glycoproteins. *J. Neurosci.* **18,** 3630–3638
12. Petrenko, A. G., Ullrich, B., Missler, M., Krasnoperov, V., Rosahl, T. W., and Südhof, T. C. (1996) Structure and evolution of neurexophilin. *J. Neurosci.* **16,** 4360–4369
13. de Wit, J., Sylwestrak, E., O'Sullivan, M. L., Otto, S., Tiglio, K., Savas, J. N., Yates, J. R., 3rd, Comoletti, D., Taylor, P., and Ghosh, A. (2009) LRRTM2 interacts with Neurexin1 and regulates excitatory synapse formation. *Neuron* **64,** 799–806
14. Ko, J., Fuccillo, M. V., Malenka, R. C., and Südhof, T. C. (2009) LRRTM2 functions as a neurexin ligand in promoting excitatory synapse formation. *Neuron* **64,** 791–798
15. Uemura, T., Lee, S. J., Yasumura, M., Takeuchi, T., Yoshida, T., Ra, M., Taguchi, R., Sakimura, K., and Mishina, M. (2010) Trans-synaptic interaction of GluRδ2 and Neurexin through Cbln1 mediates synapse formation in the cerebellum. *Cell* **141,** 1068–1079
16. Hata, Y., Davletov, B., Petrenko, A. G., Jahn, R., and Südhof, T. C. (1993) Interaction of synaptotagmin with the cytoplasmic domains of neurexins. *Neuron* **10,** 307–315
17. Hata, Y., Butz, S., and Südhof, T. C. (1996) CASK: a novel dlg/PSD95 homolog with an N-terminal calmodulin-dependent protein kinase domain identified by interaction with neurexins. *J. Neurosci.* **16,** 2488–2494
18. Biederer, T., and Südhof, T. C. (2000) Mints as adaptors. Direct binding to neurexins and recruitment of munc18. *J. Biol. Chem.* **275,** 39803–39806
19. Koroll, M., Rathjen, F. G., and Volkmer, H. (2001) The neural cell recognition molecule neurofascin interacts with syntenin-1 but not with syntenin-2, both of which reveal self-associating activity. *J. Biol. Chem.* **276,** 10646–10654
20. Song, J. Y., Ichtchenko, K., Südhof, T. C., and Brose, N. (1999) Neuroligin 1 is a postsynaptic cell-adhesion molecule of excitatory synapses. *Proc. Natl. Acad. Sci. U.S.A.* **96,** 1100–1105
21. Irie, M., Hata, Y., Takeuchi, M., Ichtchenko, K., Toyoda, A., Hirao, K., Takai, Y., Rosahl, T. W., and Südhof, T. C. (1997) Binding of neuroligins to PSD-95. *Science* **277,** 1511–1515
22. Li, Y., Zhou, Z., Zhang, X., Tong, H., Li, P., Zhang, Z. C., Jia, Z., Xie, W., and Han, J. (2013) Drosophila neuroligin 4 regulates sleep through modulating GABA transmission. *J. Neurosci.* **33,** 15545–15554
23. Sumida, M., Hong, R. M., and Tagaya, M. (1994) Role of two nucleotide-binding regions in an N-ethylmaleimide-sensitive factor involved in vesicle-mediated protein transport. *J. Biol. Chem.* **269,** 20636–20641
24. Hayashi, T., McMahon, H., Yamasaki, S., Binz, T., Hata, Y., Südhof, T. C., and Niemann, H. (1994) Synaptic vesicle membrane fusion complex: action of clostridial neurotoxins on assembly. *EMBO J.* **13,** 5051–5061
25. Söllner, T., Whiteheart, S. W., Brunner, M., Erdjument-Bromage, H., Geromanos, S., Tempst, P., and Rothman, J. E. (1993) SNAP receptors implicated in vesicle targeting and fusion. *Nature* **362,** 318–324
26. Südhof, T. C., and Rizo, J. (2011) Synaptic vesicle exocytosis. *Cold Spring Harb. Perspect. Biol.* **3,** a005637
27. Söllner, T., Bennett, M. K., Whiteheart, S. W., Scheller, R. H., and Rothman, J. E. (1993) A protein assembly-disassembly pathway *in vitro* that may correspond to sequential steps of synaptic vesicle docking, activation, and fusion. *Cell* **75,** 409–418
28. Yu, W., Kawasaki, F., and Ordway, R. W. (2011) Activity-dependent interactions of NSF and SNAP at living synapses. *Mol. Cell. Neurosci.* **47,** 19–27
29. Tian, Y., Li, T., Sun, M., Wan, D., Li, Q., Li, P., Zhang, Z. C., Han, J., and Xie, W. (2013) Neurexin regulates visual function via mediating retinoid transport to promote rhodopsin maturation. *Neuron* **77,** 311–322
30. Wang, D., Xu, M., Liu, J., Wan, Y., Deng, H., Dou, F., and Xie, W. (2006) *Drosophila* Ecp is a novel ribosome associated protein interacting with dRPL5. *Biochim. Biophys. Acta* **1760,** 1428–1433
31. Jan, L. Y., and Jan, Y. N. (1976) Properties of the larval neuromuscular junction in *Drosophila melanogaster*. *J. Physiol.* **262,** 189–214
32. van de Goor, J., Ramaswami, M., and Kelly, R. (1995) Redistribution of synaptic vesicles and their proteins in temperature-sensitive shibire(ts1) mutant *Drosophila*. *Proc. Natl. Acad. Sci. U.S.A.* **92,** 5739–5743
33. Sun, M., Xing, G., Yuan, L., Gan, G., Knight, D., With, S. I., He, C., Han, J., Zeng, X., Fang, M., Boulianne, G. L., and Xie, W. (2011) Neuroligin 2 is required for synapse development and function at the *Drosophila* neuromuscular junction. *J. Neurosci.* **31,** 687–699
34. Littleton, J. T., Chapman, E. R., Kreber, R., Garment, M. B., Carlson, S. D., and Ganetzky, B. (1998) Temperature-sensitive paralytic mutations demonstrate that synaptic exocytosis requires SNARE complex assembly and disassembly. *Neuron* **21,** 401–413
35. Rowen, L., Young, J., Birditt, B., Kaur, A., Madan, A., Philipps, D. L., Qin, S., Minx, P., Wilson, R. K., Hood, L., and Graveley, B. R. (2002) Analysis of the human neurexin genes: alternative splicing and the generation of protein diversity. *Genomics* **79,** 587–597
36. Missler, M., and Südhof, T. C. (1998) Neurexins: three genes and 1001 products. *Trends Genet.* **14,** 20–26
37. Delgado, R., Maureira, C., Oliva, C., Kidokoro, Y., and Labarca, P. (2000) Size of vesicle pools, rates of mobilization, and recycling at neuromuscular synapses of a *Drosophila* mutant, shibire. *Neuron* **28,** 941–953
38. Jahn, R., and Scheller, R. H. (2006) SNAREs–engines for membrane fusion. *Nat. Rev.* **7,** 631–643
39. Fairless, R., Masius, H., Rohlmann, A., Heupel, K., Ahmad, M., Reissner, C., Dresbach, T., and Missler, M. (2008) Polarized targeting of neurexins to synapses is regulated by their C terminal sequences. *J. Neurosci.* **28,** 12969–12981
40. Owald, D., Khorramshahi, O., Gupta, V. K., Banovic, D., Depner, H., Fouquet, W., Wichmann, C., Mertel, S., Eimer, S., Reynolds, E., Holt, M., Aberle, H., and Sigrist, S. J. (2012) Cooperation of Syd-1 with Neurexin synchronizes pre- with postsynaptic assembly. *Nat. Neurosci.* **15,** 1219–1226
41. Zhang, W., Rohlmann, A., Sargsyan, V., Aramuni, G., Hammer, R. E., Südhof, T. C., and Missler, M. (2005) Extracellular domains of α-neurexins participate in regulating synaptic transmission by selectively affecting N- and P/Q-type Ca^{2+} channels. *J. Neurosci.* **25,** 4330–4342
42. Littleton, J. T., Barnard, R. J., Titus, S. A., Slind, J., Chapman, E. R., and Ganetzky, B. (2001) SNARE-complex disassembly by NSF follows synaptic-vesicle fusion. *Proc. Natl. Acad. Sci. U.S.A.* **98,** 12233–12238
43. Tolar, L. A., and Pallanck, L. (1998) NSF function in neurotransmitter release involves rearrangement of the SNARE complex downstream of synaptic vesicle docking. *J. Neurosci.* **18,** 10250–10256
44. Lenzen, C. U., Steinmann, D., Whiteheart, S. W., and Weis, W. I. (1998) Crystal structure of the hexamerization domain of *N*-ethylmaleimide-sensitive fusion protein. *Cell* **94,** 525–536
45. Yu, R. C., Hanson, P. I., Jahn, R., and Brünger, A. T. (1998) Structure of the ATP-dependent oligomerization domain of *N*-ethylmaleimide sensitive factor complexed with ATP. *Nat. Struct. Biol.* **5,** 803–811

46. Sons, M. S., Busche, N., Strenzke, N., Moser, T., Ernsberger, U., Mooren, F. C., Zhang, W., Ahmad, M., Steffens, H., Schomburg, E. D., Plomp, J. J., and Missler, M. (2006) α-Neurexins are required for efficient transmitter release and synaptic homeostasis at the mouse neuromuscular junction. *Neuroscience* **138,** 433–446
47. Choi, Y. B., Li, H. L., Kassabov, S. R., Jin, I., Puthanveettil, S. V., Karl, K. A., Lu, Y., Kim, J. H., Bailey, C. H., and Kandel, E. R. (2011) Neurexin-neuroligin transsynaptic interaction mediates learning-related synaptic remodeling and long term facilitation in aplysia. *Neuron* **70,** 468–481
48. Aoto, J., Martinelli, D. C., Malenka, R. C., Tabuchi, K., and Südhof, T. C. (2013) Presynaptic neurexin-3 alternative splicing trans-synaptically controls postsynaptic AMPA receptor trafficking. *Cell* **154,** 75–88
49. Hanson, P. I., Roth, R., Morisaki, H., Jahn, R., and Heuser, J. E. (1997) Structure and conformational changes in NSF and its membrane receptor complexes visualized by quick-freeze/deep-etch electron microscopy. *Cell* **90,** 523–535
50. Whiteheart, S. W., Rossnagel, K., Buhrow, S. A., Brunner, M., Jaenicke, R., and Rothman, J. E. (1994) *N*-Ethylmaleimide-sensitive fusion protein: a trimeric ATPase whose hydrolysis of ATP is required for membrane fusion. *J. Cell Biol.* **126,** 945–954
51. Fleming, K. G., Hohl, T. M., Yu, R. C., Müller, S. A., Wolpensinger, B., Engel, A., Engelhardt, H., Brünger, A. T., Söllner, T. H., and Hanson, P. I. (1998) A revised model for the oligomeric state of the *N*-ethylmaleimide-sensitive fusion protein, NSF. *J. Biol. Chem.* **273,** 15675–15681
52. Tagaya, M., Wilson, D. W., Brunner, M., Arango, N., and Rothman, J. E. (1993) Domain structure of an *N*-ethylmaleimide-sensitive fusion protein involved in vesicular transport. *J. Biol. Chem.* **268,** 2662–2666
53. Ho, A., Morishita, W., Atasoy, D., Liu, X., Tabuchi, K., Hammer, R. E., Malenka, R. C., and Südhof, T. C. (2006) Genetic analysis of Mint/X11 proteins: essential presynaptic functions of a neuronal adaptor protein family. *J. Neurosci.* **26,** 13089–13101
54. Atasoy, D., Schoch, S., Ho, A., Nadasy, K. A., Liu, X., Zhang, W., Mukherjee, K., Nosyreva, E. D., Fernandez-Chacon, R., Missler, M., Kavalali, E. T., and Südhof, T. C. (2007) Deletion of CASK in mice is lethal and impairs synaptic function. *Proc. Natl. Acad. Sci. U.S.A.* **104,** 2525–2530
55. Gokce, O., and Südhof, T. C. (2013) Membrane-tethered monomeric neurexin LNS-domain triggers synapse formation. *J. Neurosci.* **33,** 14617–14628
56. Biederer, T., and Sudhof, T. C. (2001) CASK and protein 4.1 support F-actin nucleation on neurexins. *J. Biol. Chem.* **276,** 47869–47876
57. Wojcik, S. M., and Brose, N. (2007) Regulation of membrane fusion in synaptic excitation-secretion coupling: speed and accuracy matter. *Neuron* **55,** 11–24
58. Kawasaki, F., and Ordway, R. W. (2009) Molecular mechanisms determining conserved properties of short term synaptic depression revealed in NSF and SNAP-25 conditional mutants. *Proc. Natl. Acad. Sci. U.S.A.* **106,** 14658–14663
59. Nagiec, E. E., Bernstein, A., and Whiteheart, S. W. (1995) Each domain of the N-ethylmaleimide-sensitive fusion protein contributes to its transport activity. *J. Biol. Chem.* **270,** 29182–29188